RESEARCH ARTICLE VOLCANICA

Unrest at the Nevados de Chillán volcanic complex: a failed or yet to unfold magmatic eruption?

Yves Moussallam*[αβ], Philipson Bani[β], C. Ian Schipper[γ], Carlos Cardona[δ], Luis Franco[δ], Talfan Barnie[ε], Álvaro Amigo[δ], Aaron Curtis[ζ], Nial Peters[α], Alessandro Aiuppa[ηθ], Gaetano Giudice[θ], Clive Oppenheimer[α]

[α] *Department of Geography, University of Cambridge, Downing Place, Cambridge, CB2 3EN, United Kingdom.*
**Full list of affiliations given in Affiliations section.*

Abstract

New eruptive activity at volcanoes that have been long quiescent poses a significant challenge to hazard assessment, as it requires assessment of how the situation may develop. Such incipient activity is often poorly characterised as most quiescent volcanoes are poorly monitored, especially with respect to gas geochemistry. Here, we report gas composition and flux measurements from a new vent at the onset of eruptive activity at the Nevados de Chillán volcanic complex (Chile) in January-February 2016. The molar proportions of H_2O, CO_2, SO_2, H_2S and H_2 gases are found to be 98.4, 0.97, 0.11, 0.01 and 0.5 mol % respectively. The mean SO_2 flux recorded in early February 2016 during periods of eruptive discharge amounts to 0.4–0.6 kg s^{-1}. We show that magmatic gases were involved in this activity, associated with a sequence of eruptions. Tephra ejected by the first blast of 8 January are dominated by lithic fragments of dacitic composition. By contrast the tephra ejected from a subsequent eruption contains both lithic fragments of dense dacite, and a fresher, sparsely vesicular material of basaltic andesite composition. By October 2017, the ejected tephra was again dominated by dense dacitic lithic material. Together with seismic and ground deformation evidence, these observations suggest that a small intrusion of basaltic to andesitic magma at shallow level led to the explosive activity. Our serendipitous survey, right at the onset of eruptive activity, provides a valuable window into the processes of reawakening of a dormant volcano.

Keywords: `Volcanic gases; Volcanic unrest; Eruption trigger; UV camera; Multi-Gas; Trail By Fire`

1 Introduction

Nevados de Chillán, a large volcanic complex built in the Southern Volcanic Zone of the Chilean Andes is formed along a 12 km northwest-trending ridge (Figure 1. It is considered one of the most hazardous volcanoes in Chile due to the proximity of the resort towns of Las Trancas and Termas de Chillán—approximately 10 and 5 km away from the active crater, respectively—with permanent populations of 1600 rising to 30,000 during the high season. Whilst Holocene activity is represented by widespread pyroclastic flow and tephra fall deposits around the volcano, lahars associated with snow melt are considered to be the greatest potential hazard [Orozco et al. 2016]. In particular, the Las Trancas valley is covered with repeated sequences of lahar deposits separated by paleosols and intercalated with centimetre-thick pyroclastic flow deposits [Carrasco and Andrés 2012]. The latest hazard map shows high lahar threats extending more than 50 km away from the complex [Orozco et al. 2016]. A new episode of unrest began at the 3212-m-high volcanic complex in December 2015, followed shortly by an eruptive episode between 8 January and 3 May 2016. Here we investigate the onset of this activity so as to assess its origins and possible development. We present the results of (i) in-situ gas composition measurements made on 13 January 2016, within days of the first eruption, (ii) remotely sensed measurements of SO_2 flux obtained on 2 February 2015, and (iii) compositional (bulk and glass) analyses of tephra emitted by the 8 January 2016 and two subsequent eruptions, one shortly before 3 February 2016 and a second on 11 October 2017.

1.1 Volcanic context

Activity at Nevados de Chillán dates back at least ca 640 ka with extrusion of subglacial andesite flows, followed by subglacial and subaerial eruption of basaltic andesite to low-silica rhyolite lavas, and the emplacement of ignimbrites ca 40 ka ago [Dixon et al. 1999]. Since then, the activity has been focused at two centres 6 km apart; the predominantly andesitic Cerro Blanco subcomplex [Mee et al. 2009] and the more silicic Las Termas subcomplex [Deruelle and Deruelle 1974; Dixon et al. 1999].

In recent years, the Las Termas subcomplex has

*Corresponding author: yves.moussallam@gmail.com

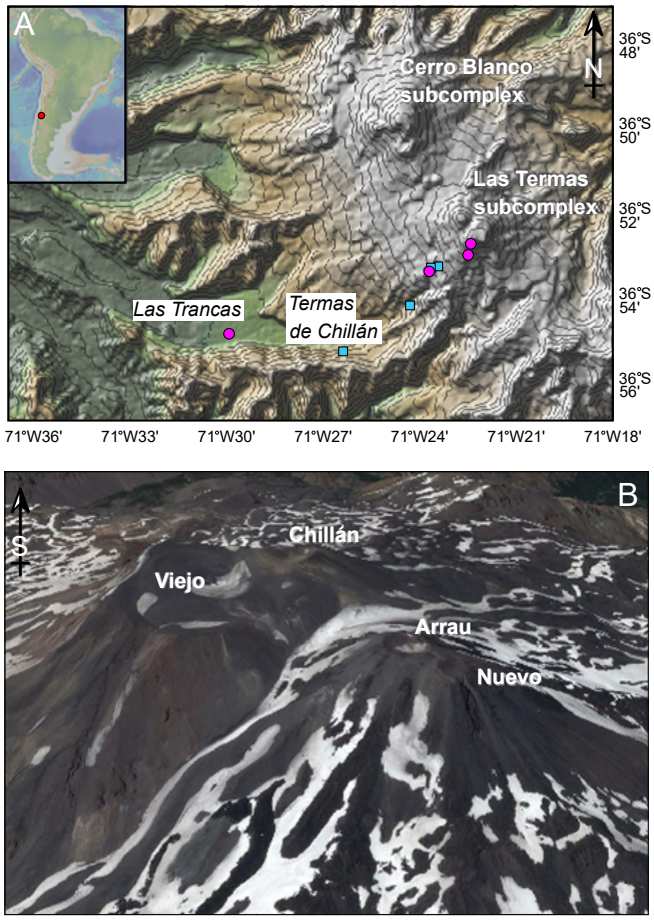

Figure 1: [A] DEM of the Nevados de Chillán Volcanic Complex. The Cerro Blanco and Las Termas subcomplexes are visible together with the surrounding valleys in which lahar and pyroclastic flow hazards are concentrated. The towns of Las Trancas and Termas de Chillán are shown. Contour lines are drawn every 100 meters and go from 3200 to 600 m. Purple circles show the location of tephra samples. Blue squares show the location of site used for remote sensing observations with UV cameras. [B] Google Earth view of the Las Termas subcomplex looking south at the Nuevo, Arrau, Viejo and Chill an cones (image: Centre National d'étude spatial, 3 January 2014, 4 km eye altitude). Map data: Google, DigitalGlobe ©2018, CNES/ Airbus ©2018.

been the most active. This subcomplex comprises four cones, Nuevo, Arrau, Viejo and Chillán (from north to south; Figure 1). Viejo is the oldest stratocone, it was active from ca 9.3 ka to 2270 BP and is composed of interstratified lavas and pyroclastic units that include prominent densely welded andesite and dacite agglutinate layers [Dixon et al. 1999]. Chillán cone is located south-west of Viejo and partially overlaps it. It is a dacitic cone dominated by lavas intercalated with pyroclastic deposits, and its last eruption took place in 1883 [Brüggen 1948] possibly associated with the collapse of the southern flank of the edifice [Naranjo et al. 2008]. Nuevo and Arrau are dacitic lava cones that formed on top of the older volcán Democrático. Nuevo formed from 1906 to 1943 while Arrau formed from 1973 to 1986 [Deruelle 1977; Dixon et al. 1999; Naranjo et al. 1994].

From August to September 2003, a series of low-magnitude explosive events generated gas and ash columns 400 to 500 m high, leaving a 64 m double crater in the saddle between the Nuevo and Arrau cones [Naranjo and Lara 2004]. On 29 January 2009, the Volcanic Ash Advisory Centre of Buenos Aires reported a small ash column rising 500 m above the volcanic complex. This eruption could not be confirmed by subsequent field observations, which found instead that an unnoticed eruption must have occurred between January and August 2008, producing a new lava field termed Volcán Sebastián, 1 km northeast of the Arrau cone [Naranjo and Moreno 2009].

1.2 The 2015–present unrest

In December 2015, the Observatorio Volcanológico de Los Andes del Sur (OVDAS), part of the Servicio Nacional de Geología y Minería (SERNAGEOMIN), changed the warning level from green to yellow following an increase in seismicity observed during the month prior. On 8 January 2016 at 17:56 local time, an eruption occurred at Nevados de Chillán producing a small column of ash. On 13 January 2016, the authors observed a new vent, 30 m across (Figure 2A). On 14 and 15 January 2016, two more eruptions occurred, and several hundred further small eruptions have been recorded up to the time of writing (December 2017) [SERNAGEOMIN 2017].

On 29 January 2016, a second vent, 25–30 m wide, opened, followed by a third in early February 2016 along a NNE trend Figure 2B–C). The proximity of these vents precluded unambiguous identification of which was responsible for the frequent small eruptions. On 9 May, 8 August and 1 September 2016, three comparatively larger eruptions (in terms of plume height) occurred, producing ash clouds up to 2000 m above the vent and resulting in a widening of the 8 January vent Figure 2D). A fourth vent opened in October 2016 (Figure 2E), eventually merging with the first and third in March 2017 to produce a large crater more than 100 m across. This is the likely source of the activity occurring at the time of writing (December 2017). From March 2016, incandescence has been sporadically reported during night-time eruptions, and sustained weak incandescence was reported between 25 and 31 March 2017 [SERNAGEOMIN 2017]. All eruptions have been characterised by columns of gases and ash of low height (<2 km) with most of the erupted material deposited within 1 km of the crater. Figure 3 summarises seismic and other routine observations made by OVDAS - SERNAGEOMIN, showing the evolution of unrest since its onset. Of note is the significant episode of volcanic tremor at the onset of activity [SERNAGEOMIN 2017].

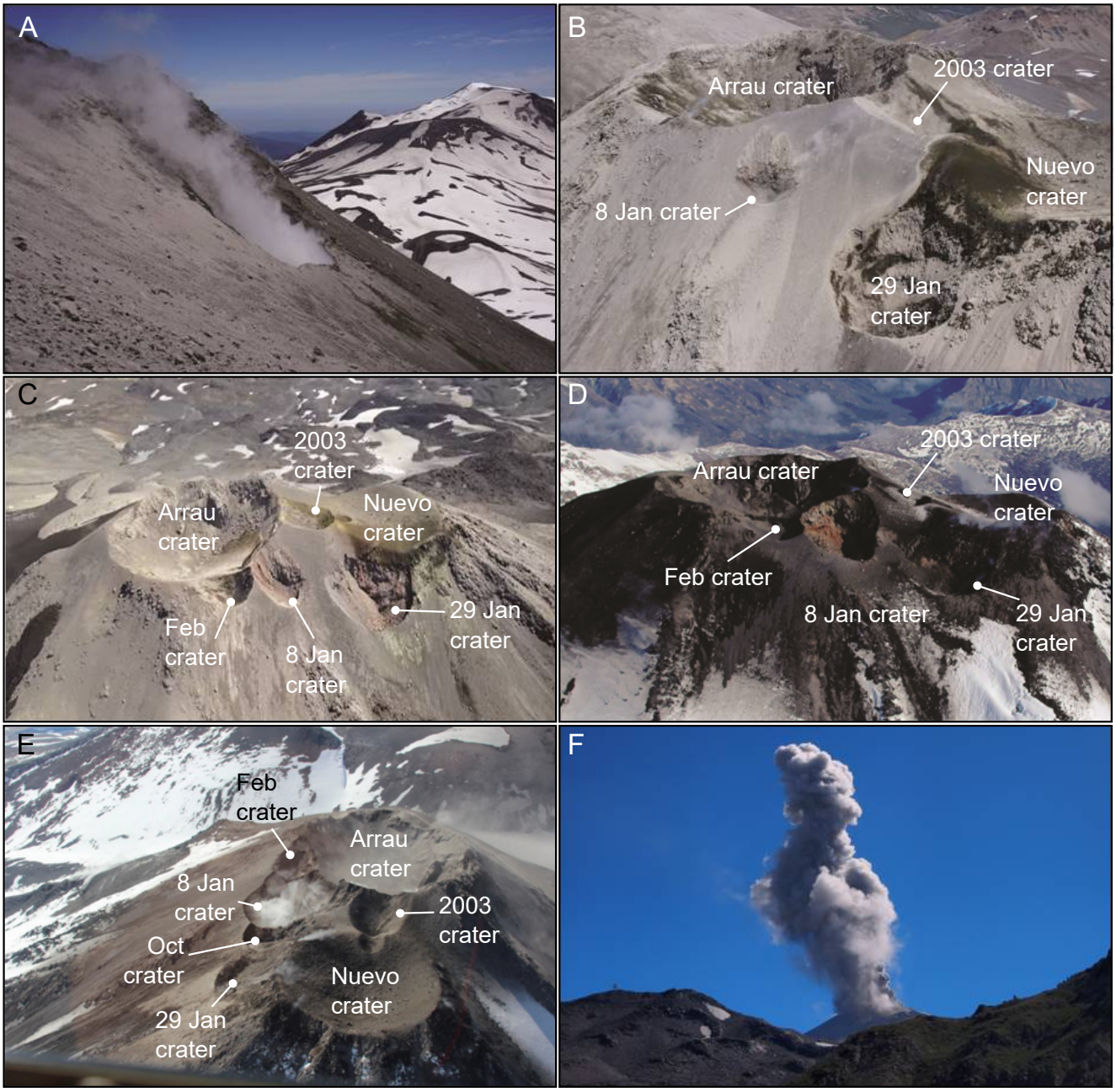

Figure 2: [A] Photograph of the first crater, 30 m across, formed on 8 January 2016. The photograph was taken on 13 January 2016, looking north-east. [B] Aerial photograph taken on 30 January 2016, looking south, showing the first and second craters (formed 29 January 2016). [C] Aerial photograph taken on 11 February 2016, looking south-west, showing the first, second and third craters (formed sometime between 30 January and 11 February 2016). [D] Aerial photograph taken on 9 August 2016, looking south-south-west, showing the growth of the first crater following a comparatively larger eruption that produce a 2000 m high ash plume. [E] Aerial photograph taken on 22 October 2016, looking south-east, showing the first, second, third and fourth craters (formed sometime in October 2016). [F] Photograph of an eruption taken on the 2 February 2016.

2 Methods

2.1 In-situ gas measurements

Gas composition data were obtained on 13 January 2016, five days after the first eruption. The data were collected using a portable "Multi-GAS" instrument [Shinohara 2005] deployed a few meters downwind of the first vent, which was actively degassing at the time (S36°52'1.64"; W71°22'40.18"; Figure 2A). The instrument incorporated SO_2, H_2S and H_2 electrochemical sensors. The SO_2 and H_2 sensors have calibration ranges of 0–200 ppmv while the H_2S sensor has a calibration range of 0–100 ppmv. A non-dispersive infrared sensor was used for CO_2 and calibrated for 0–10,000 ppmv with an accuracy ±2 %. A relative humidity (*Rh*) sensor (Galltec) was used to measure H_2O, providing a measuring range of 0–100 % *Rh* with an accuracy of ± 2 %. The conversion from relative humidity to water mixing ratio was made following Buck [1981] and using the following equation:

$$H_2O = \frac{\left\{ \begin{array}{l} 6.1121 \times (1.0007 + 3.46 \times P^{-6}) \\ \quad \times \exp\left[\frac{17.502 \times T}{240.97 + T}\right] \times \left[\frac{Rh}{100} \times 10^6\right] \end{array} \right\}}{P} \quad (1)$$

where H_2O is the absolute water mixing ratio in ppmv, T is temperature in °C, *Rh* is relative humidity in %, and P is atmospheric pressure in mbar. The gas temperature used in this equation is measured in real time by the Multi-GAS, the pressure is also measured by the Multi-GAS and the average during the measurements is used. All sensors were housed inside a weatherproof box, with the ambient air sampled via Teflon tubing connected to a HEPA filter fed through an inlet in the box and circulated via a miniature 12V rotary pump through the sensors. An on-board data-logger captured measurements at a rate of 1 Hz. The complete system was powered by a small (6 Ah) 12V LiPo battery. Similar systems have now been deployed at many volcanoes and the system used here is the same as that reported in Moussallam et al. [2016].

All sensors were calibrated in the laboratory at INGV Palermo (in October 2015), with target gases of known amount. The differences in response time for the different sensors were corrected by finding the lag times from correlation analysis of the various time series (see Moussallam et al. [2014] for sensors response time). Post processing was performed using Ratiocalc [Tamburello 2015]. Below we report H_2O, H_2 and CO_2 mixing ratios after correction for mean ambient air mixing ratios (measured by the Multi-GAS directly prior to entering the plume). The measured H_2S mixing ratio is corrected for a laboratory-determined cross-sensitivity with SO_2 gas (amounting to 16%).

2.2 UV camera

SO_2 emissions from Nevados de Chillán were observed with two Apogee Alta U260 ultraviolet cameras on the 13, 30, 31 of January and on 2, 3 of February 2016. On 13 January 2016, the UV camera system was located 3 km away from the vent at S36°53'23.42"; W 71°23'49.56". On 30 January 2016, the UV camera system was located 8 km away from the vent at S36°55'01.89"; W71°26'37.68". On 31 January 2016, the UV camera system was located 2.7 km away from the vent at S36°53'08.76"; W71°23'57,25". On 2 February 2016, the UV camera system was located 5 km away from the vent at S36°54'14.80"; W71°24'12,71". On 3 February 2016, the UV camera system was located 2.5 km away from the vent at S36°53'17.32"; W71°23'35.54".

The ultraviolet cameras were coupled to Pentax B2528-UV lenses, with focal length of 25 mm (FOV 24°), and 10 nm full width at half maximum (FWHM) bandpass filters were placed immediately in front of each lens one filter was centred at 310 nm (Asahi Spectra XBPA310) where SO_2 absorbs and the other at 330 nm (XBPA330) outside the SO_2 absorption region [Kantzas et al. 2010; Mori and Burton 2006]. Image acquisition and processing were achieved using Vulcamera [Tamburello et al. 2011]. Every image acquired is saved in a 24 bit Portable Network Graphics (png) file with lossless compression. A set of four SO_2 calibration cells were used (94, 189, 475 and 982 ppm·m) to calibrate the apparent absorbance [Kantzas et al. 2010]. Two parallel sections in our data series, perpendicular to the plume transport direction were used to derive plume speed (ranging from 3 to 7 m s^{-1}, with an average of 6 m s^{-1}). The data processing was carried out following the protocols outlined Kantzas et al. [2010].

2.3 Tephra analysis

Two tephra samples were collected on 13 January 2016 at S36°52'8.1097"; W71°22'38.1298" and S36°52'24.6853"; W71°22'41.7828". Both samples were collected on snow that was clean before the 8 January eruption and hence originate from ash fall produced by the first eruption. The first sample consists predominantly of fine ash (< 63 µm), while the second consists predominantly of coarse ash (< 2 mm). A third tephra sample was collected on 3 February 2016 at: S36°53.291' W071°23.606' from a patch of snow that was clean on 13 January 2016. The sample hence originates from ash fall from an eruption that occurred between 14 January and 3 February 2016. A fourth tephra sample was collected on 11 October 2017 at S36°54.808' W071°29.574' directly from ash fall in the village of Las Trancas. Given that the samples were collected opportunistically, and in very small amounts, no attempt to quantify grain sizes was attempted.

Tephra samples were analysed for bulk composi-

Table 1 – Chronology of the 2016–ongoing unrest and induced morphological change to the summit area.

Date (dd-mm-yy)	
31-Dec-15	Alert level changed from green to yellow following increased seismic activity
08-Jan-16	First eruption of ash at 17:56 local time. First new crater formed.
09-Jan-16	At least nine small eruptions
29-Jan-16	First eruption from the second crater.
11-Feb-16	Identification of a third crater (formed in February)
Mar-16	First report of incandescence during eruptions at night
09-May-16	Larger eruption emitting ash 1700 m high
08-Aug-16	Larger eruption emitting ash 2000 m high
01-Sep-16	Largest eruption recorded to date
22-Oct-16	Identification of a fourth crater (formed in October)
20-Jan-17	Union of the first and third craters
07-Mar-17	Start of a new eruptive phase with one eruption reaching 1600 m high
15-Mar-17	Union of the fourth crater with the first and third
24-Mar-17	Sustained, low-intensity incandescence reported during five consecutive nights

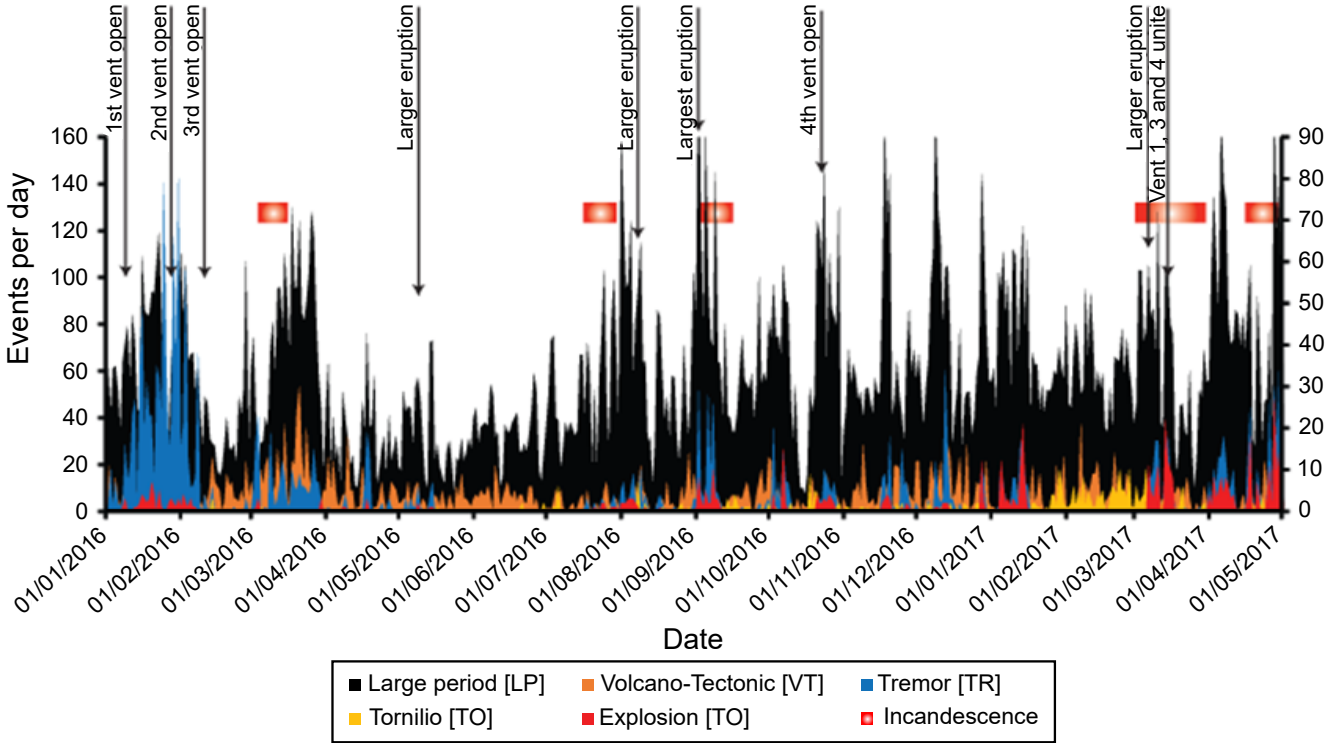

Figure 3: Time series showing the evolution of seismic events for the period of 1 January 2016 to 1 April 2017. Large period events are reported on the left vertical axis while volcano-tectonic, tremor, tornillo and explosions are reported on the right vertical axis. Periods of reported incandescence and specific events are indicated.

tion by Inductively Coupled Plasma–Atomic Emission Spectrometry (ICP–AES) at the Laboratoire Magmas et Volcans (Clermont-Ferrand). Ash particles were examined and analysed for major element chemistry using backscatter electron (BSE) microscopy and electron microprobe (EPMA) analysis on a five-spectrometer JEOL JXA-8230 Superprobe at Victoria University of Wellington. Glass analyses were performed using 15 kV, 8.0 nA, and a defocussed beam of 10 µm. To mitigate for Na loss, Na was measured first in the analytical sequence, at reduced count times (10 s on peak; 5 s background) at a fixed peak position. Major elements were standardized against rhyolitic (VG568) and basaltic (VGA-99) glasses and pure oxides of Ti, Mn and Cr [Jarosewich et al. 1980]. Analytical spots were chosen to avoid microlites, thus capturing evolved interstitial glasses.

3 Results

3.1 Gas composition

We obtained 12 minutes of high quality Multi-GAS measurements. Data acquisition time was restricted due to the unstable nature of the vent area (requiring rope access), and the need to limit time exposed in a hazardous area. Multi-GAS measurements are presented in Figure 4, which shows four scatter plots of CO_2; H_2O; H_2S and H_2 vs. SO_2 mixing ratios in the plume emitted from the first vent. The strong positive co-variations observed between SO_2 and the other detected volatiles confirm a single, common, volcanic origin. The gas/SO_2 molar plume ratios were obtained from the gradients of the best-fit regression lines. Scatter plots yield the following molar ratios: CO_2/SO_2 of 9.1 ± 1.3, H_2O/SO_2 of 925 ± 97, H_2S/SO_2 of 0.13 ± 0.03 and H_2/SO_2 of 4.74 ± 0.56. Together these data yield proportions of H_2O, CO_2, SO_2, H_2S and H_2 of 98.4, 0.97, 0.11, 0.01 and 0.5 mol % (Table 2). The CO_2, H_2O, H_2S and H_2 vs. SO_2 yield correlations with R^2 value of 0.77, 0.83, 0.47 and 0.77, respectively.

3.2 SO_2 flux

The ultraviolet cameras were deployed at distances of 2.5 km (03 February 2016), 2.7 km (31 Jan. 2016), 3 km (13 Jan. 2016), 5 km (02 February 2016) and 8 km (30 Jan. 2016) from the source. Weather conditions during these measurements were generally good, with long periods of clear sky, except on 3 February, which was cloudy. Results obtained over these 5 days of measurements indicate a negligible SO_2 flux outside eruptive episodes. For instance, on 13, 30 and 31 January there were no eruptions during the observation periods, and the recordings did not register any SO_2 release, despite the generally short distances between the UV cameras and the active crater. Eruptions did occur during measurement periods on 2 and 3 February. However, due to heavy cloud on 3 February, only the data collected on 2 February are useful. On that day, UV camera measurements were taken downwind of the active crater after most of the ash in the eruptive plume had deposited. Figure 5 shows the SO_2 emission rate obtained during two eruptions on 2 February. The emissions fluctuate between 0.1 and 1 kg s^{-1} with a mean value of 0.5 kg s^{-1}. These fluctuations of SO_2 emission rate are associated with observable successive pulses during the eruptive discharge period. High resolution videos of eruptions on 2 and 3 February are given in the supplementary material.

3.3 Tephra composition

Bulk tephra compositions are given in Table 3. Clear differences can be seen between the bulk composition of the tephra emitted during the first eruption on 8 January and that of the subsequent ash fall (occurring between 13 January and 3 February). In the total alkali-silica diagram, 8 January tephra are dacitic, while the subsequent tephra are andesitic Figure 6A). When examined by backscattered electrons (BSE), both samples of the 8 January tephra are similar, and consist of glassy, dense material with 30–40 % plagioclase microlites (Figure 6B). In all samples, some of the dacitic fragments are bounded by corroded vesicles containing vapour-phase SiO_2 polymorphs (Figure 6D). Microstructural phase identification of these SiO_2 crystals is beyond the scope of this work, but many of them show the "fishscale cracking" that is diagnostic of α-cristobalite that has undergone volume contraction during the $\beta - \alpha$ transition [Horwell et al. 2013]. These same ash fragments also have devitrified groundmass containing SiO_2 polymorphs (Figure 6D) that we have not structurally identified, but that are similar to groundmass cristobalite in the holocrystalline cores of effusive silicic lava bodies [Schipper et al. 2015]. The small amount of cristobalite (and SiO_2 assumed to be cristobalite) is all intimately bound to glass and/or other crystal phases, and is therefore unlikely to pose any respiratory hazard at Chillán [Horwell et al. 2012], but it is rather an indicator that at least some of the dacitic ash fragments is derived from lava bodies extensively degassed at low pressure, under slow-cooling conditions [Schipper et al. 2017]. Interstitial glass in the dacitic material is rhyolitic (Figure 6A). Similar materials are present in the subsequent ash fall, but with an additional component that is moderately vesicular, with fewer microlites, and with interstitial glass of andesitic composition (Figure 6). No alteration products and/or hydrothermal minerals were observed in any of the ash samples.

4 Discussion

4.1 Magmatic-gas propelled phreatic eruptions

The composition of the gases emitted from the first 2016 vent at Chillán was measured five days after the first eruption. Subsequent images of the summit area show that the vent was later buried by tephra and that passive outgassing had ceased (Figure 2). Assuming a gas mixture at equilibrium, following Giggenbach [1987] and Giggenbach [1996] and using the thermodynamic data of Stull et al. [1969], the gas-melt equilibrium temperature and oxygen fugacity (fO_2) can be calculated using:

$$\log \frac{H_2}{H_2O} = -\frac{12707}{T} + 2.548 - \frac{1}{2}\log fO_2 \qquad (2)$$

and

$$\log \frac{SO_2}{H_2S} = \frac{27377}{T} - 3.986 + \frac{3}{2}\log fO_2 - \log fH_2O. \qquad (3)$$

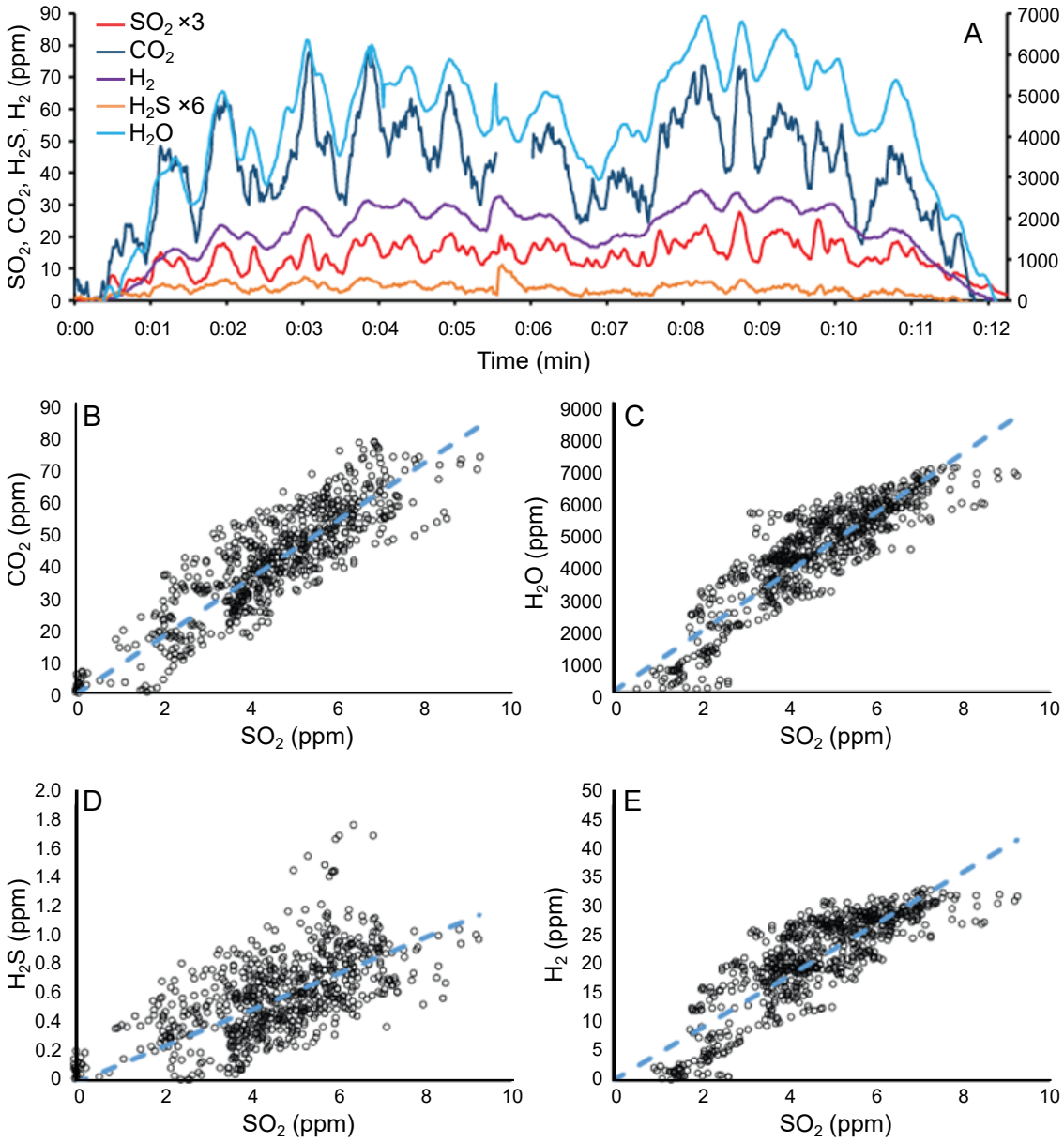

Figure 4: [A] Plume mixing ratios measurements taken on 13 January 2016 for 12 min at an acquisition frequency of 1 Hz. All data are after correction of background atmospheric amounts. Note that in [A], H_2O is reported on the right vertical axis while other gases are reported on the left axis. The small data gap in the CO_2 sensor is due to removal of a 30 s period where the operator approached the unit, which has recorded exhaled breath. [B]–[E] Scatter plots of the mixing ratios of [B] CO_2, [C] H_2O, [D] H_2S and [E] H_2 vs SO_2 in the Chillán plume. Least-square regression lines are shown in dashed blue on each plot.

These yield an equilibrium temperature of 856 °C and a $\log fO_2$ equivalent to ΔQFM = +0.6 (where QFM refers to the quartz-fayalite-magnetite buffer, and where $\Delta QFM = \log fO_2 - \log fO_2$ of QFM at corresponding temperature) or ΔNNO = -0.2 (where NNO refers to the Nickel Nickel-Oxide buffer, and where $\Delta NNO = \log fO_2 - \log fO_2$ of NNO at corresponding temperature). Error on the measured gas ratios results in asymmetrical uncertainty of -58 and +30 °C on the equilibrium temperature and of -0.1 and +0.2 log units on the deviation from the QFM or NNO buffer. Equations for the QFM and NNO buffer used here are from Frost [1991]. The value of fH_2O used here is 0.98 given that at 1 bar the fugacity of a gas is equal to its partial pressure and that $P_{H_2O} = (P_{tot} \times n_{H_2O})/n_{tot} = 0.98$ bar.

The dominance of SO_2 over H_2S and the high equilibrium temperature strongly support a magmatic origin for the gas emitted by the first 2016 vent. The computed equilibrium temperature of 856 °C is much higher than the temperature at which scrubbing of magmatic gases by hydrothermal systems is expected to be significant [Gerlach et al. 2008; Symonds et al. 2001],

Table 2 – X/SO_2 molar and mass ratios measured by Multi-GAS and gas composition of the plume at Chillán volcano. Error are expressed as the standard error of the regression analysis and subsequent error propagation.

Gas	Mixed plume molar ratio (X/SO_2)	Error ($1\ \sigma$)	Mixed plume mass ratio (X/SO_2)	Error ($1\ \sigma$)	Mixed plume composition (mol %)	Error ($1\ \sigma$)
H_2O	925	97	260	27	98	10
CO_2	9.1	1.3	6.3	0.9	1.0	0.1
SO_2	1	0	1	1	0.1	0
H_2S	0.13	0.03	0.07	0.02	0.01	0.003
H_2	4.74	0.560	0.14915	0.01762	0.504	0.060

Table 3 – ICP–AES bulk composition of tephra samples. The first two samples were collected on 13 January and originate from ash fall produced by the first eruption on 8 January 2013. The third sample was collected on 3 February 2016, the eruption date producing this ash fall is unknown but constrained between 13 January and 3 February 2016. The fourth originate from an ash fall during an eruption on 11 October 2017. Note the significant difference in composition between the third sample and the others.

wt %	13 January 2016 S1	13 January 2016 S2	03 February 2016	11 October 2017
SiO_2	67.51	66.57	61.9	64.48
Al_2O_3	14.57	14.97	15.93	15.70
Fe_2O_3	4.79	4.86	6.16	5.60
MgO	1.27	1.21	2.53	1.85
CaO	2.67	2.8	4.58	3.88
Na_2O	4.45	4.13	4.11	3.44
K_2O	2.48	2.14	2.02	2.09
TiO_2	0.88	0.92	0.99	1.03
MnO	0.09	0.09	0.11	0.11
P_2O_5	0.2	0.21	0.24	0.21
Ba	0.0499	0.0442	0.0463	0.06
Sr	0.0245	0.0277	0.0367	0.04
H_2O^+	0.17	0.43	0.26	0.47
H_2O^-	0.31	1.02	0.63	0.19
Total	99.44	99.43	99.53	99.15

giving confidence that the reported gas composition has not been affected by secondary processes other than cooling. The equilibrium temperature, whilst a minimum estimate of the magmatic temperature, is consistent with equilibrium with a dacitic to basaltic andesite magma at depth. The clear magmatic composition of the gas at the very onset of eruptive activity implies that the hundreds of small eruptions that have occurred at Chillán since, are not driven by a hydrothermal system but are instead propelled by pressurised magmatic gases.

A large hydrothermal system with hot springs, fumaroles and hot grounds is present at the Nevados de Chillán Volcanic Complex. The most significant fumaroles are located near the village of Termas de Chillán, where water derived from hot springs is used for the spa of the same name. Other nearby locations with hydrothermal activity include the Valle Hermoso and Aguas Caliente sectors. In all locations, fumaroles and hot springs have maximum temperatures around 90 °C [Berríos Guerra 2015]. Our observations suggest that this large hydrothermal system was largely bypassed by the recent activity.

4.2 A shallow level magmatic intrusion

At the onset of eruptive activity, a single dacitic component was present in the erupted tephra (Figure 6). This probably originates from the Arrau lava cone, made of glassy block-flow medium-Si dacites [66.6–67.6 % SiO_2: Dixon et al. 1999]. In the following days, a second basaltic-andesite component appeared in the erupted tephra. It can be difficult to identify juvenile components in the material from small eruptions that may incorporate a variety of lithics [Pardo et al. 2014], and the probable origin of this second

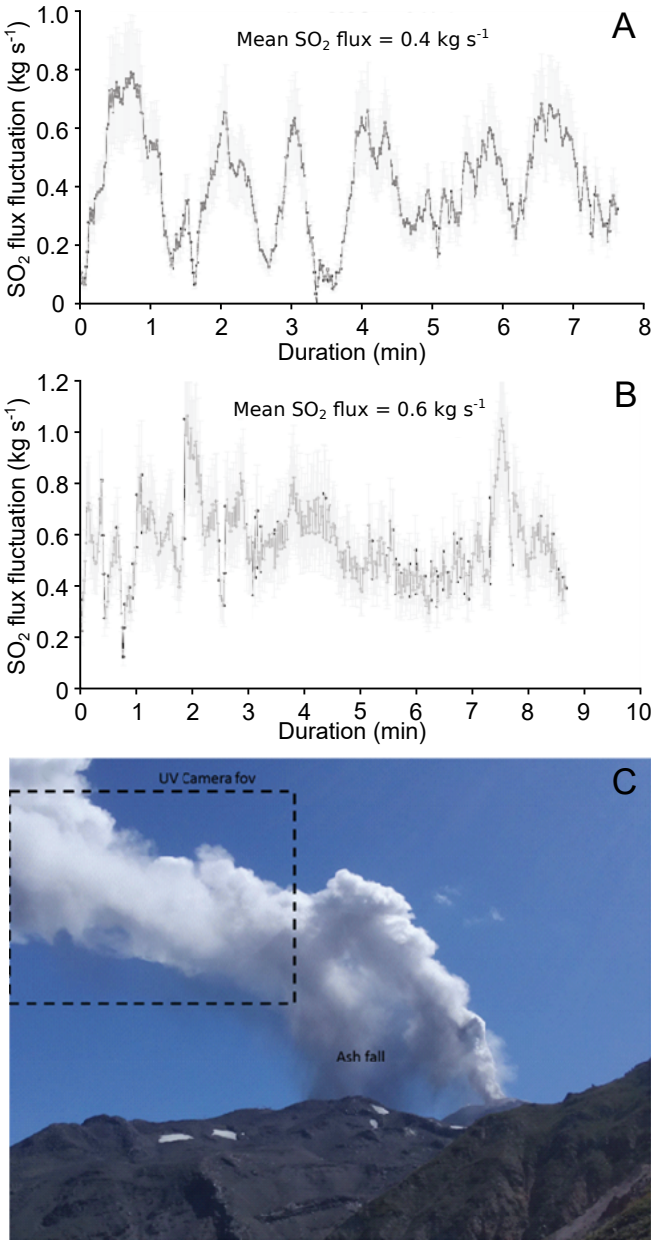

Figure 5: SO_2 flux time series obtained during two periods of eruptive discharge ([A] and [B]) at Nevados de Chillán on 2 February 2016 as measured by UV cameras. [C] location of the UV camera field of view, measuring SO_2 absorption after most of the ash contained in the plume has separated. The full eruption—which is composed of several pulses—can been seen in the supplementary video.

component cannot be readily ascertained since basaltic andesites are well-represented in the stratigraphy of Nevados de Chillán. However, these are much more common at Cerro Blanco than the currently active Las Termas subcomplexes, and we consider it less likely that these fragments are lithics recycled from the pre-existing volcanic edifice—especially considering they disappeared from the mix of ejected material by October 2017. Although the fragments are vesicular and appear unaltered (Figure 6C) they cannot be confirmed as juvenile. What is clear is that the gas emitted during the repeated eruptions originates from exsolution from a melt at high temperature (> 850 °C). These elevated temperatures are consistent with the incandescence observed during night-time eruptions, reported intermittently by OVDAS–SERNAGEOMIN since March 2016.

These observations suggest the presence of magma at a shallow level within the edifice. This is corroborated by seismicity recorded by OVDAS–SERNAGEOMIN with long period (LP) events located at depths less than 5 km. The significant tremor registered in the first few days of the new activity suggests magma or fluids motion at that time. Several periods of increased tremor have been recorded since, many temporally associated with explosions and incandescence (Figure 3). Altogether, these observations suggest that the current eruptive activity was triggered by the rise and shallow emplacement of magma, accompanied by exsolution of volatiles triggering explosions that opened a new vent and ejected fragments of the cone. The activity since might have been sustained by periodic small-scale recharge and/or gas exsolution from the cooling and crystallising magma (Figure 7). The surficial expression of the intrusion, with several craters aligned along a straight NNE line (Figure 2B–C), is consistent with diking. The size of the intrusion is unknown, but we note the lack of evidence for deformation that has been monitored by GPS and tiltmeter stations from OVDAS–SERNAGEOMIN and using interferometric synthetic aperture radar observations (unpublished data). Given the evidence for a shallow intrusion, this tends to suggest it has a comparatively small volume.

4.3 Scenarios for evolution of the eruption

With nearly two years since the onset of activity and with continued daily to monthly eruptive events at the time of writing (December 2017), it remains pressing to address the evolution of this episode of activity. However, our conceptual model for the intrusion (Figure 7) provides little basis for prognostication of how the episode will unfold. Nevertheless, we can pose three scenarios: The first is a gradual or abrupt end of the unrest with the intrusion stalling at shallow level without a magmatic eruption. This "failed magmatic eruption" scenario [Moran et al. 2011] is statistically likely, considering that globally, most recorded periods of phreatic eruptions at volcanoes are not followed by magmatic eruptions [Barberi et al. 1992]. Examples of such "failed eruptions" include the 1979–1982 unrest at Mt Ontake, Japan [Oikawa 2008] and the 2006–2007 unrest at Fourpeaked volcano, USA [Gardine et al. 2011].

The second scenario considers a transition to a magmatic eruption. In this case, the intrusion does reach the surface and lava is extruded either effusively or explosively (or both). Well documented examples in-

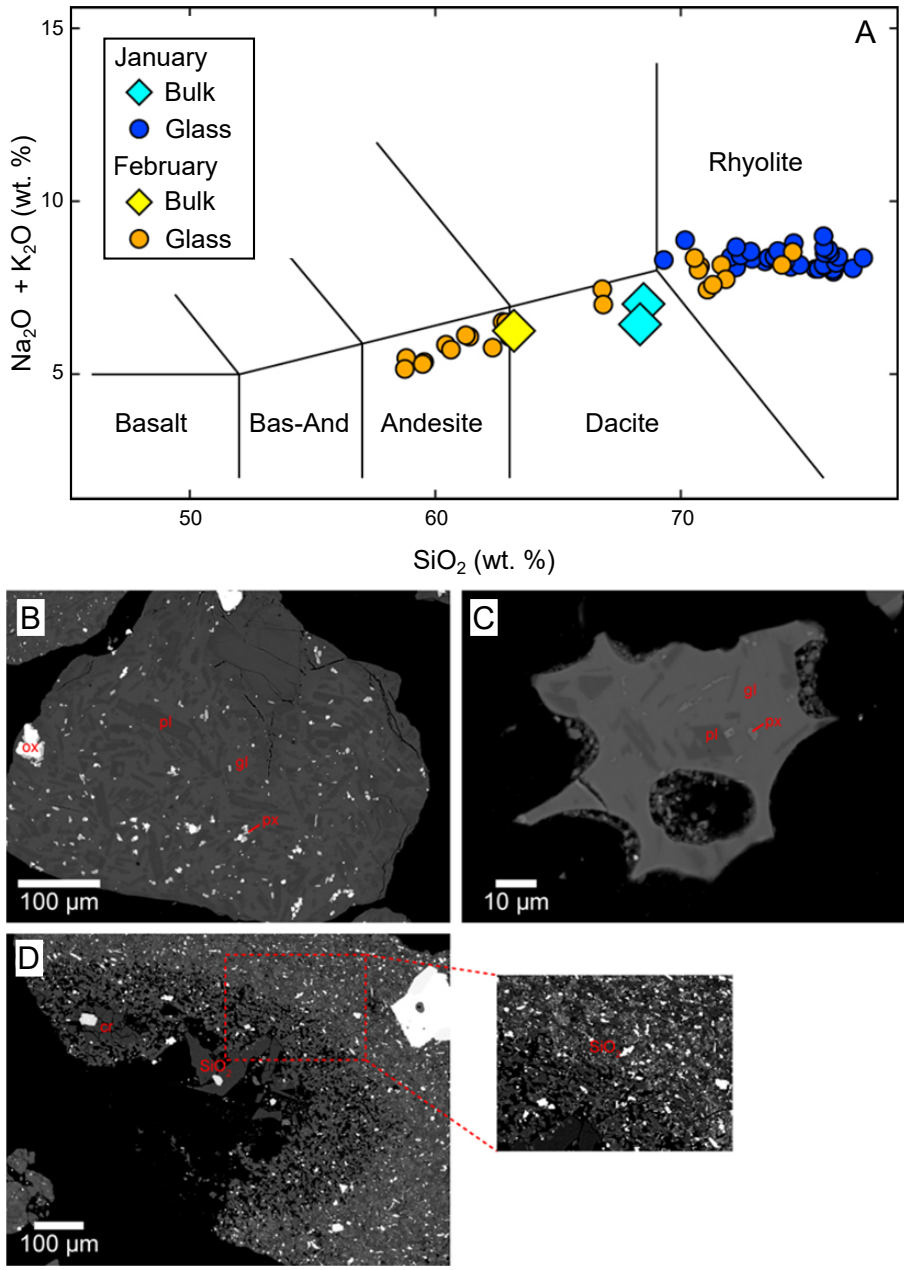

Figure 6: Textures and geochemistry of tephra. [A] Total alkali-silica diagram showing the compositions of bulk tephra samples (Table 3) and interstitial glass within grains. [B]–[C] BSE images of tephra fragments showing the dacitic material that dominated the 8 January blast material and 11 October material [B], and the andesitic component that is also present in the February blast material [C]. Components are marked glass (gl), plagioclase (pl), pyroxene (px), and oxides (ox). [D] BSE image of SiO_2 polymorph-bearing dacite from 8 January. Note that ash grain is bounded by a SiO_2-bearing vesicle, around which the walls are corroded. One SiO_2 grain shows fishscale cracking that is diagnostic of cristobalite. Expanded view with high-contrast colour balance shows devitrified groundmass, in which the darkest grey phase is an unidentified SiO_2 polymorph.

clude the 1980 eruption of Mt St Helens, preceded by two months of earthquakes and frequent phreatic explosions [Lipman and Mullineaux 1981] and the 1990–1995 eruption at Unzen volcano, where seismicity and phreatic eruptions escalated over a year, culminating in the extrusion of a lava dome and generation of pyroclastic flows [Nakada et al. 1999].

Between these two possibilities lies a third scenario in which activity could continue at a low level for several years. Such prolonged activity, induced by shallow magmatic intrusions, accompanied by magmatic degassing but with limited expulsion of juvenile tephra or lava, has characterized eruptions of Turrialba [2010 to present: Campion et al. 2012; Moussallam et al. 2014; Rizzo et al. 2016] and Copahue [2012 to present: Caselli et al. 2015; Tamburello 2015; Tassi et al. 2017].

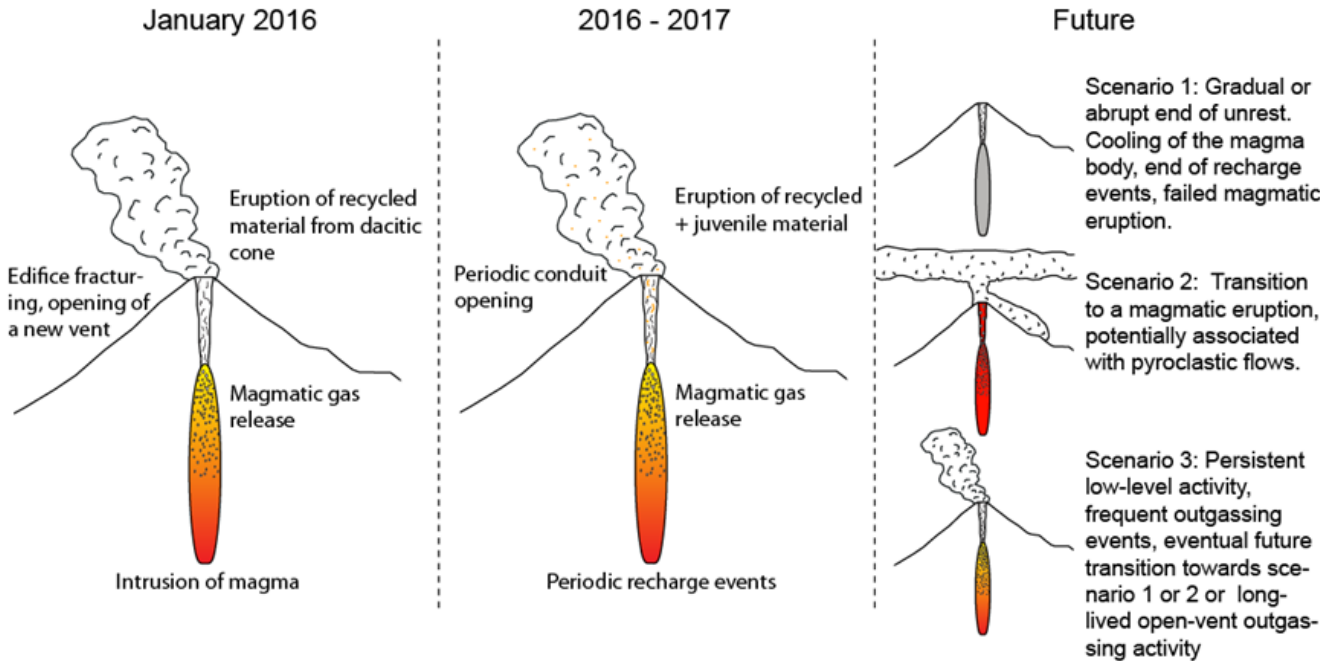

Figure 7: Schematic cross-section of the past, current and potential future configurations of the volcanic system.

5 Conclusions

In 2016, we measured the composition of gases emitted at the onset of the ongoing (at the time of writing in December 2017) eruptive episode at Nevados de Chillán. We also measured the SO_2 flux emission during eruptive discharge and the composition of tephra associated with these explosive events. The main conclusions we derive from this study are:

1. Right from the onset, eruptive activity was driven by magmatic gases, although ejecta were dominated by recycled material from the edifice.
2. A shallow magmatic intrusion is likely to be the trigger for the current unrest and may be periodically recharged.

Acknowledgements

We thank René Cárdenas, Monchy Zapata, Corinne Bentley and the entire Cuerpo de Socorro Andino de Chile, session Las Trancas for their invaluable logistical help, essential in collecting the data presented here. This research was conducted as part of the "Trail By Fire" expedition (PI: Y. Moussallam). The project was supported by the Royal Geographical Society (with the Institute of British Geographers) with the Land Rover Bursary; the Deep Carbon Observatory DECADE Initiative; Ocean Optics; Crowcon; Air Liquide; Thermo Fisher Scientific; Santander; Cactus Outdoor; Santander; Turbo Ace and Team Black Sheep. We thank Sebastien Carretier and Rose-Marie Ojeda together with IRD South-America personnel for all their logistical help. Y.M. acknowledges support from the Leverhulme Trust. C.I.S. acknowledges a research startup grant from Victoria University of Wellington. C.O. is supported by the NERC Centre for the Observation and Modelling of Earthquakes, Volcanoes and Tectonics. A.A. acknowledges the ERC grant no. 305377 (BRIDGE). We are grateful to Jamie Farquharson, Nick Varley and an anonymous reviewer for comments which improved the quality of this manuscript.

Author affiliations

α Department of Geography, University of Cambridge, Downing Place, Cambridge, CB2 3EN, United Kingdom.
β Université Clermont Auvergne, CNRS, IRD, OPGC, Laboratoire Magmas et Volcans, F-63000 Clermont-Ferrand, France.
γ School of Geography, Environment and Earth Sciences, Victoria University of Wellington, PO Box 600, Wellington 6140, New Zealand.
δ Observatorio Vulcanológico de los Andes del Sur, Servicio Nacional de Geología y Minería, Temuco, 03850, Chile.
ε Nordic Volcanological Center, Institute of Earth Sciences, Sturlugata 7 – Askja, 101 Reykjavik, Iceland.
ζ Jet Propulsion Laboratory-California Institute of Technology, 4800 Oak Grove Drive, Pasadena, CA 91109, USA.
η Dipartimento DiSTeM, Università di Palermo, Via archirafi 36, 90146, Palermo, Italy.
θ Istituto Nazionale di Geofisica e Vulcanologia, Sezione di Palermo Via La Malfa, 153, 90146, Palermo, Italy.

Author contributions

Y.M., P.B., C.I.S., C.C., L.F., T.B., Á.A., A.C. contributed to acquiring data presented in this manuscript. A.A and G.G contributed the Multi-GAS instrument. All authors participated in discussions and writing of the manuscript.

Data availability

Raw data presented here are not available. Supplementary video files can be found alongside the online version of this article. Supplementary video 1: Eruption on 2 February 2016; Supplementary video 2: Eruption on 3 February 2016; Supplementary video 3: View of Nevados de Chillán from Las Trancas on 1 February 2016.

Copyright notice

References

Barberi, F., A. Bertagnini, P. Landi, and C. Principe (1992). "A review on phreatic eruptions and their precursors". *Journal of Volcanology and Geothermal Research* 52.4, pp. 231–246. DOI: 10.1016/0377-0273(92)90046-g.

Berríos Guerra, C. A. (2015). "Caracterización Geoquímica de Sistemas Geotermales en Zonas de Transición: Volcanes Nevados de Chillán y Copahue". PhD thesis. Santiago de Chile: Universidad de Chile, Facultad de Ciencias Físicas y Matemáticas. Departamento de Geología.

Brüggen, J. (1948). "Contribución a la geología de los volcanes y Termas de Chillán."

Buck, A. L. (1981). "New Equations for Computing Vapor Pressure and Enhancement Factor". *Journal of Applied Meteorology* 20.12, pp. 1527–1532. DOI: 10.1175/1520-0450(1981)020<1527:nefcvp>2.0.co;2.

Campion, R., M. Martinez-Cruz, T. Lecocq, C. Caudron, J. Pacheco, G. Pinardi, C. Hermans, S. Carn, and A. Bernard (2012). "Space- and ground-based measurements of sulphur dioxide emissions from Turrialba Volcano (Costa Rica)". *Bulletin of Volcanology* 74.7, pp. 1757–1770. DOI: 10.1007/s00445-012-0631-z.

Carrasco, R. and I. Andrés (2012). "Estudio de la dinámica de los lahares recientes del flanco oeste del complejo volcánico Nevados de Chillán (36°50'S), Andes del Sur".

Caselli, A., M. Agusto, M. L. Velez, P. Forte, C. Bengoa, R. Daga, J. M. Albite, and B. Capaccioni (2015). "The 2012 Eruption". *Active Volcanoes of the World*. Springer Berlin Heidelberg, pp. 61–77. DOI: 10.1007/978-3-662-48005-2_4.

Deruelle, B. (1977). "Sur l'activité recente des Nevados de Chillán (Chili Central)". *Comptes Rendus de l'Academie des Sciences de Paris* 284, pp. 1651–1654.

Deruelle, B. and J. Deruelle (1974). "Los volcanes Cuaternarios de los Nevados de Chillán (Chile central) y reseña sobre el volcanismo Cuaternario de los Andes Chilenos". *Estudios geológicos* 30.2, pp. 97–108.

Dixon, H. J., M. D. Murphy, S. J. Sparks, R. Chávez, J. A. Naranjo, P. N. Dunkley, S. R. Young, J. S. Gilbert, and M. R. Pringle (1999). "The geology of Nevados de Chillán volcano, Chile". *Revista geológica de Chile* 26.2. DOI: 10.4067/s0716-02081999000200006.

Frost, B. R. (1991). "Introduction to oxygen fugacity and its petrologic importance". *Reviews in Mineralogy and Geochemistry* 25.1, pp. 1–9.

Gardine, M., M. West, C. Werner, and M. Doukas (2011). "Evidence of magma intrusion at Fourpeaked volcano, Alaska in 2006–2007 from a rapid-response seismic network and volcanic gases". *Journal of Volcanology and Geothermal Research* 200.3-4, pp. 192–200. DOI: 10.1016/j.jvolgeores.2010.11.018.

Gerlach, T. M., K. A. McGee, and M. P. Doukas (2008). *Emission rates of CO_2, SO_2, and H_2S, scrubbing, and preeruption excess volatiles at Mount St. Helens, 2004–2005: Chapter 26 in A volcano rekindled: the renewed eruption of Mount St. Helens, 2004-2006*. Tech. rep. US Geological Survey.

Giggenbach, W. F. (1996). "Chemical Composition of Volcanic Gases". *Monitoring and Mitigation of Volcano Hazards*. Springer Berlin Heidelberg, pp. 221–256. DOI: 10.1007/978-3-642-80087-0_7.

Giggenbach, W. (1987). "Redox processes governing the chemistry of fumarolic gas discharges from White Island, New Zealand". *Applied Geochemistry* 2.2, pp. 143–161. DOI: 10.1016/0883-2927(87)90030-8.

Horwell, C. J., B. J. Williamson, E. W. Llewellin, D. E. Damby, and J. S. L. Blond (2013). "The nature and formation of cristobalite at the Soufrière Hills volcano, Montserrat: implications for the petrology and stability of silicic lava domes". *Bulletin of Volcanology* 75.3. DOI: 10.1007/s00445-013-0696-3.

Horwell, C. J., B. J. Williamson, K. Donaldson, J. S. L. Blond, D. E. Damby, and L. Bowen (2012). "The structure of volcanic cristobalite in relation to its toxicity; relevance for the variable crystalline silica hazard". *Particle and Fibre Toxicology* 9.1, p. 44. DOI: 10.1186/1743-8977-9-44.

Jarosewich, E., J. Nelen, and J. A. Norberg (1980). "Reference Samples for Electron Microprobe Analysis". *Geostandards and Geoanalytical Research* 4.1, pp. 43–47. DOI: 10.1111/j.1751-908x.1980.tb00273.x.

Kantzas, E. P., A. McGonigle, G. Tamburello, A. Aiuppa, and R. G. Bryant (2010). "Protocols for UV camera volcanic SO2 measurements". *Journal of Volcanology and Geothermal Research* 194.1-3, pp. 55–60. doi: 10.1016/j.jvolgeores.2010.05.003.

Lipman, P. W. and D. R. Mullineaux (1981). *The 1980 eruptions of Mount St. Helens, Washington*. 1250. US Dept. of the Interior, US Geological Survey.

Mee, K., J. S. Gilbert, D. W. McGarvie, J. A. Naranjo, and M. S. Pringle (2009). "Palaeoenvironment reconstruction, volcanic evolution and geochronology of the Cerro Blanco subcomplex, Nevados de Chillán volcanic complex, central Chile". *Bulletin of Volcanology* 71.8, pp. 933–952. doi: 10.1007/s00445-009-0277-7.

Moran, S. C., C. Newhall, and D. C. Roman (2011). "Failed magmatic eruptions: late-stage cessation of magma ascent". *Bulletin of Volcanology* 73.2, pp. 115–122. doi: 10.1007/s00445-010-0444-x.

Mori, T. and M. Burton (2006). "The SO2camera: A simple, fast and cheap method for ground-based imaging of SO2in volcanic plumes". *Geophysical Research Letters* 33.24. doi: 10.1029/2006gl027916.

Moussallam, Y., N. Peters, C. Ramírez, C. Oppenheimer, A. Aiuppa, and G. Giudice (2014). "Characterisation of the magmatic signature in gas emissions from Turrialba Volcano, Costa Rica". *Solid Earth* 5.2, pp. 1341–1350. doi: 10.5194/se-5-1341-2014.

Moussallam, Y., P. Bani, A. Curtis, T. Barnie, M. Moussallam, N. Peters, C. I. Schipper, A. Aiuppa, G. Giudice, Á. Amigo, G. Velasquez, and C. Cardona (2016). "Sustaining persistent lava lakes: Observations from high-resolution gas measurements at Villarrica volcano, Chile". *Earth and Planetary Science Letters* 454, pp. 237–247. doi: 10.1016/j.epsl.2016.09.012.

Nakada, S., H. Shimizu, and K. Ohta (1999). "Overview of the 1990–1995 eruption at Unzen Volcano". *Journal of Volcanology and Geothermal Research* 89.1-4, pp. 1–22. doi: 10.1016/s0377-0273(98)00118-8.

Naranjo, J., R. Chávez, R. Sparks, J. Gilbert, and P. Dunkley (1994). "Nuevos antecedentes sobre la evolución Cuaternaria del Complejo Volcánico Nevados de Chillán". *Congreso Geológico Chileno*. Concepción, Chile, pp. 342–345.

Naranjo, J., J. S. Gilbert, and R. Sparks (2008). *Geología del complejo volcánico Nevados de Chillán, Région del Biobío. Servicio Nacional Geología y Minería, Carta Geología de Chile, Serie Geología Básica, mapa escala 1: 50,000, Santiago*. Tech. rep. 114.

Naranjo, J. and H. Moreno (2009). "Reciente erupción en el Complejo Volcánico Nevados de Chillán, Región del Biobío". *XII Congreso Geológico Chileno, Santiago, Actas*. Vol. 3, p. 016.

Naranjo, J. A. and L. E. Lara (2004). "August-September 2003 small vulcanian eruption at the Nevados de Chillán Volcanic Complex (36°50'S), Southern Andes (Chile)". *Revista geológica de Chile* 31.2. doi: 10.4067/s0716-02082004000200011.

Oikawa, T. (2008). "Reinvestigation of the historical eruption and fumarolic activity records at Ontake Volcano, central Japan. Misunderstanding reports about the 774 AD and 1892 AD eruptions". *Bulletin of the Geological Survey of Japan* 59.5/6, pp. 203–210. doi: 10.9795/bullgsj.59.203.

Orozco, G., G. Jara, and D. Bertin (2016). *Peligros del complejo volcánico Nevados de Chillán, Région del Biobío. Servicio Nacional Geología y Minería, Carta Geología de Chile, Serie Geología Básica, mapa escala 1: 50,000, Santiago*. Tech. rep. 28.

Pardo, N. et al. (2014). "Perils in distinguishing phreatic from phreatomagmatic ash; insights into the eruption mechanisms of the 6 August 2012 Mt. Tongariro eruption, New Zealand". *Journal of Volcanology and Geothermal Research* 286, pp. 397–414. doi: 10.1016/j.jvolgeores.2014.05.001.

Rizzo, A. L., A. D. Piazza, J. M. de Moor, G. E. Alvarado, G. Avard, M. L. Carapezza, and M. M. Mora (2016). "Eruptive activity at Turrialba volcano (Costa Rica): Inferences from 3He/4He in fumarole gases and chemistry of the products ejected during 2014 and 2015". *Geochemistry, Geophysics, Geosystems* 17.11, pp. 4478–4494. doi: 10.1002/2016gc006525.

Schipper, C. I., J. M. Castro, H. Tuffen, F. B. Wadsworth, D. Chappell, A. E. Pantoja, M. P. Simpson, and E. C. L. Ru (2015). "Cristobalite in the 2011–2012 Cordón Caulle eruption (Chile)". *Bulletin of Volcanology* 77.5. doi: 10.1007/s00445-015-0925-z.

Schipper, C. I., C. Mandon, A. Maksimenko, J. M. Castro, C. E. Conway, P. Hauer, M. Kirilova, and G. Kilgour (2017). "Vapor-phase cristobalite as a durable indicator of magmatic pore structure and halogen degassing: an example from White Island volcano (New Zealand)". *Bulletin of Volcanology* 79.10. doi: 10.1007/s00445-017-1157-1.

SERNAGEOMIN (2017). *Nevados de Chillán*. url: http://www.sernageomin.cl/complejo-volcanico-nevados-de-chillan (visited on 04/26/2018).

Shinohara, H. (2005). "A new technique to estimate volcanic gas composition: plume measurements with a portable multi-sensor system". *Journal of Volcanology and Geothermal Research* 143.4, pp. 319–333. doi: 10.1016/j.jvolgeores.2004.12.004.

Stull, D. R., E. F. Westrum, and G. C. Sinke (1969). *The chemical thermodynamics of organic compounds*. J. Wiley New York.

Symonds, R., T. Gerlach, and M. Reed (2001). "Magmatic gas scrubbing: implications for volcano monitoring". *Journal of Volcanology and Geothermal Research* 108.1-4, pp. 303–341. doi: 10.1016/s0377-0273(00)00292-4.

Tamburello, G. (2015). "Ratiocalc: Software for processing data from multicomponent volcanic gas analyzers". *Computers & Geosciences* 82, pp. 63–67. doi: 10.1016/j.cageo.2015.05.004.

Tamburello, G., E. P. Kantzas, A. J. S.McGonigle, and A. Aiuppa (2011). "Vulcamera: a program for measuring volcanic SO_2 using UV cameras". *Annals of Geophysics* 54.2. ISSN: 2037-416X. DOI: 10.4401/ag-5181.

Tassi, F., M. Agusto, C. Lamberti, A. T. Caselli, G. Pecoraino, C. Caponi, J. Szentiványi, S. Venturi, and O. Vaselli (2017). "The 2012–2016 eruptive cycle at Copahue volcano (Argentina) versus the peripheral gas manifestations: hints from the chemical and isotopic features of fumarolic fluids". *Bulletin of Volcanology* 79.10. DOI: 10.1007/s00445-017-1151-7.